ACS OMEGA

http://pubs.acs.org/journal/acsodf

Article

Electronic Inhomogeneity Influence on the Anomalous Hall Resistivity Loops of $SrRuO_3$ Epitaxially Interfaced with 5d Perovskites

Lena Wysocki, Jörg Schöpf, Michael Ziese, Lin Yang, András Kovács, Lei Jin, Rolf B. Versteeg, Andrea Bliesener, Felix Gunkel, Lior Kornblum, Regina Dittmann, Paul H. M. van Loosdrecht, and Ionela Lindfors-Vrejoiu*

Cite This: *ACS Omega* 2020, 5, 5824−5833

Read Online

ACCESS | Metrics & More | Article Recommendations | Supporting Information

ABSTRACT: $SrRuO_3$, a 4d ferromagnet with multiple Weyl nodes at the Fermi level, offers a rich playground to design epitaxial heterostructures and superlattices with fascinating magnetic and magnetotransport properties. Interfacing ultrathin $SrRuO_3$ layers with large spin−orbit coupling 5d transition-metal oxides, such as $SrIrO_3$, results in pronounced peaklike anomalies in the magnetic field dependence of the Hall resistivity. Such anomalies have been attributed either to the formation of Néel-type skyrmions or to modifications of the Berry curvature of the topologically nontrivial conduction bands near the Fermi level of $SrRuO_3$. Here, epitaxial multilayers based on $SrRuO_3$ interfaced with 5d perovskite oxides, such as $SrIrO_3$ and $SrHfO_3$, were studied. This work focuses on the magnetotransport properties of the multilayers, aiming to unravel the role played by the interfaces with 5d perovskites in the peaklike anomalies of the Hall resistance loops of $SrRuO_3$ layers. Interfacing with large band gap insulating $SrHfO_3$ layers did not influence the anomalous Hall resistance loops, while interfacing with the nominally paramagnetic semimetal $SrIrO_3$ resulted in pronounced peaklike anomalies, which have been lately attributed to a topological Hall effect contribution as a result of skyrmions. This interpretation is, however, under strong debate and lately alternative causes, such as inhomogeneity of the thickness and the electronic properties of the $SrRuO_3$ layers, have been considered. Aligned with these latter proposals, our findings reveal the central role played in the anomalies of the Hall resistivity loops by electronic inhomogeneity of $SrRuO_3$ layers due to the interfacing with semimetallic 5d^5 $SrIrO_3$.

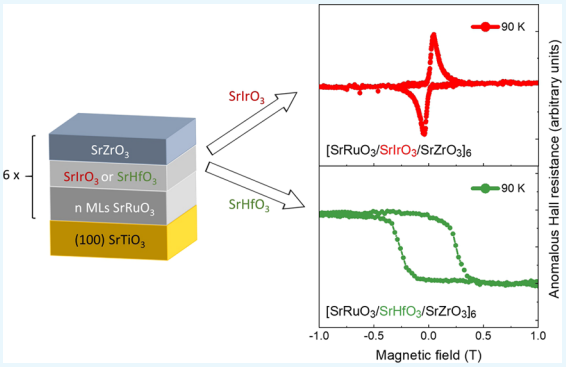

1. INTRODUCTION

Epitaxial heterostructures and superlattices of perovskite oxides have become a fascinating playground for solid-state physics researchers over the past two decades. Tailoring physical properties by heterostructuring dissimilar perovskites, to yield functionalities that do not exist in the single compounds, has been the main driving force behind the efforts to master the epitaxial growth of perovskite oxides. Lately, there is a strongly motivated turn of attention toward 5d materials with large spin−orbit coupling (SOC)-dominated properties and this has been impacting the research of perovskite superlattices as well.[1−3] A highly appealing prospect has been that the proximity of the 5d ions with large SOC to a ferromagnet in a heterostructure that breaks the inversion symmetry may result in a strong Dzyaloshinskii−Moriya interaction (DMI). If the resulting interfacial DMI is on a competitive footing with the magnetocrystalline anisotropy and the Heisenberg exchange interaction of the ferromagnet, noncollinear magnetic structures with nontrivial topology can be stabilized in heterostructures or multilayers. The heterostructure scenario, which has been highly successful to generate nontrivial magnetic textures for metal multilayers, may be tested also for perovskite superlattices. Moreover, the prospect of forming skyrmions in epitaxial oxide heterostructures is very exciting, as electric field effects may be employed to generate and/or manipulate skyrmions.

Over the last couple of years, studies on magnetotransport properties of epitaxial ultrathin heterostructures involving the 4d transition-metal oxide $SrRuO_3$ (SRO) and the 5d semimetal $SrIrO_3$ have sparked great interest, ignited by the proposal that very small skyrmions (i.e., about 10 nm diameter)[4−6] or noncoplanar magnetic textures[3] can form in ultrathin ferromagnetic $SrRuO_3$ layers interfaced with the large spin−

Received: November 24, 2019
Accepted: February 5, 2020
Published: March 10, 2020

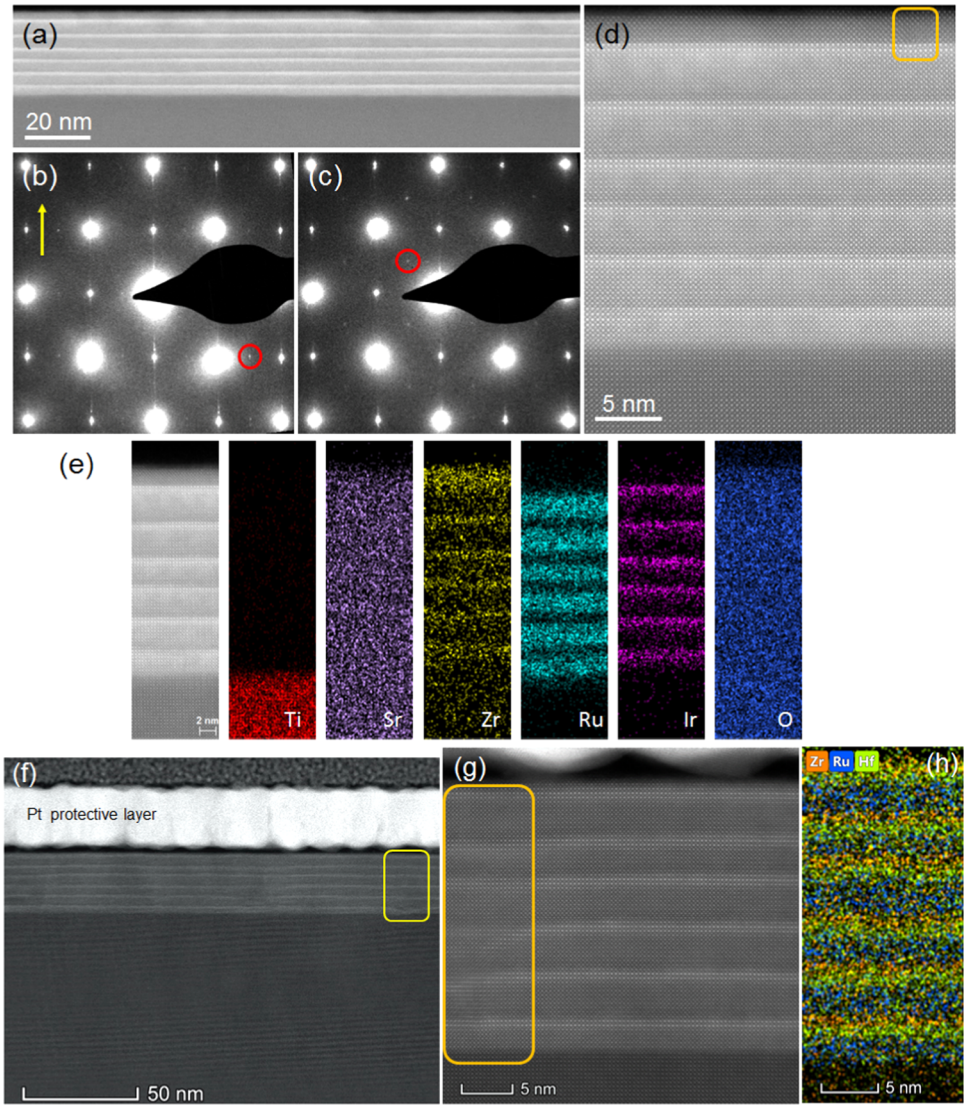

Figure 1. Microstructure investigations by HAADF-STEM, SAED, and EDXS of $SrZrO_3/SrRuO_3/SrIrO_3$ (a–e) and $SrZrO_3/SrRuO_3/SrHfO_3$ (f–h) multilayers, with nominally 6 ML-thick $SrRuO_3$ layers (samples 6RIZ and 6RHZ). The overview STEM micrographs in (a) and (f) show that the layers are uniform. The high-magnification micrographs in (d) and (g) highlight the quality of the interfaces for both types of multilayers. SAED patterns (displayed in (b) and (c)) acquired by the transmission electron microscope allowed us to observe reflections related to orthorhombic distortion (marked by red circles). The yellow arrow in (b) marks the growth direction of multilayers. EDXS elemental mapping images across the entire stacks with six repeats of the individual layers of the two multilayers are shown in (e) and (h).

orbit coupling $SrIrO_3$, as a result of a strong interfacial DMI. The formation of skyrmions was primarily inferred from the observation of anomalies in the anomalous Hall effect (AHE) resistivity loops resembling contributions from a topological Hall effect (THE),[7] which appeared in a range around the temperature at which the anomalous Hall constant changes sign.[4,8] However, the origin of these unconventional features is still under debate. Recently, the anomalies were attributed to spatial,[8] structural,[9] or electronic[10] sample inhomogeneities that impact the anomalous Hall effect by modifications of the band structure.

Here, we studied a set of multilayers and heterostructures, in which we interfaced the ferromagnetic $SrRuO_3$ with the 4d band insulator $SrZrO_3$ and, on the other side, with the 5d $SrIrO_3$ or with the 5d band insulator $SrHfO_3$. Such asymmetric multilayers break the inversion symmetry at both top and bottom interfaces of the ferromagnetic layer. We were motivated to grow these complex multilayers by the expectation that in epitaxial $SrIrO_3/SrRuO_3/SrZrO_3$ multilayers the possibly resulting interfacial DMI can be enhanced if additive DMI can be obtained due to DMI of opposite signs at the top and bottom interfaces, similar to the way in which DMI arises for metallic dipolar-coupled asymmetric multilayers of Pt/Co/Ir or Pt/Co/Ta.[11,12] DMI was experimentally and theoretically well studied and proved for metallic multilayers,[12] but no similar studies of DMI at epitaxial oxide interfaces have been published so far. The magnitude of interfacial DMI at the $SrRuO_3/SrIrO_3$ interface was addressed by preliminary calculations in ref 4, predicting a DMI of a magnitude able to yield 10 nm small skyrmions. A large interfacial DMI can significantly reduce the size of the magnetic domains with nontrivial topology. Furthermore, the increased magnetic volume in multilayers may reinforce the stability of metastable magnetic domains against thermal fluctuations and thus expand their temperature stability range closer to the Curie temperature of $SrRuO_3$ layers. However, as we will show later,

https://dx.doi.org/10.1021/acsomega.9b03996
ACS Omega 2020, 5, 5824−5833

it is unlikely that the anomalies observed in the Hall effect resistivity loops are caused by skyrmions.

In the second part of this study, the role played by the electronic structure of the 5d perovskite oxide $SrIrO_3$ in the overall anomalous Hall resistivity loops of the heterostructures was addressed by substituting the strong SOC paramagnetic semimetal $SrIrO_3$ ($5d^5$ Ir ion) with the band insulator $SrHfO_3$ ($5d^0$ Hf ion). Unconventional anomalies resembling a THE contribution were found only in all of the multilayers in which $SrRuO_3$ was interfaced with $SrIrO_3$ but not when $SrIrO_3$ was replaced with insulating $SrHfO_3$.

2. RESULTS AND DISCUSSION

A summary of the microstructural investigations by high-angle annular dark-field scanning transmission electron microscopy (HAADF-STEM) and high-resolution energy-dispersive X-ray spectroscopy (EDXS) of two multilayers is presented in Figure 1, showing low-magnification overview micrographs in Figure 1a,f. The multilayer 6RIZ, possessing $SrRuO_3/SrIrO_3$ interfaces, is compared to the multilayer 6RHZ where the $SrRuO_3$ is interfaced with $SrHfO_3$ instead of $SrIrO_3$ (see Table 1 for their description). The imaged multilayers exhibit good uniformity and thicknesses, matching the expected thickness values from the monitoring by reflective high-energy electron diffraction (RHEED) during their growth (see the Supporting Information). The five different perovskites that we employ here, $SrTiO_3$ (STO), $SrRuO_3$, $SrIrO_3$, $SrHfO_3$, and $SrZrO_3$, have at room temperature (RT) pseudocubic lattice parameters increasing between 3.905 Å (for $SrTiO_3$) and ≈4.13 Å (for $SrZrO_3$ that has the largest pseudocubic lattice parameter from the five perovskites under study), resulting in compressive epitaxial strain values of up to about 6%.[13] Therefore, strain relaxation is expected to occur, e.g., by formation of structural domains and/or structural defects, such as misfit dislocations. For example, orthorhombic domains with the long orthorhombic *c* axis oriented in-plane in two perpendicular directions could be detected for multilayer 6RIZ by selective area electron diffraction (SAED), taken during transmission electron microscopy (TEM) imaging of the specimen (see the SAED patterns in Figure 1b,c). We note that at room temperature (RT) all of the bulk compounds under study, except the cubic $SrTiO_3$, have an orthorhombic structure (*Pbnm* space group). The characteristic reflections yielded by orthorhombic distortions (due to A-site atom displacements in Figure 1b and to oxygen octahedral rotations in Figure 1c) of the perovskite layers are marked by the red circles. Additionally, misfit dislocations were found in the upper part of the 6RIZ multilayer, for example, in the top right area marked in Figure 1d by the yellow rectangle, at the interface between the $SrIrO_3$ layer and the topmost $SrZrO_3$ capping layer. In the case of sample 6RHZ, misfit dislocations form already in the lower part of the multilayer: sample 6RHZ has larger levels of epitaxial misfit strain, as $SrHfO_3$ (pseudocubic lattice parameter ≈4.07 Å[14]) has a significantly larger lattice parameter than that of $SrIrO_3$ (pseudocubic lattice parameter ≈3.96 Å[15]) and relatively large defects propagate through the whole stack, as marked in Figure 1f,g. For zoomed-in HAADF-STEM images of the defects marked by yellow rectangles, see Figure S2, Supporting Information. High-resolution EDXS enabled us to observe the distribution of the B-site cations (i.e., Ru, Ir/Hf, and Zr) in the individual layers of the two different multilayers (Figure 1e,h), and the spatial extent of these cations matches the expected layer thickness based on the RHEED monitoring of the individual layer growth. The three-component layer sequence was preserved across the entire multilayer (see Figure 1h).

Table 1. Nomenclature and Description of the Investigated Samples and the Curie Temperature, T_C, of Their Ferromagnetic $SrRuO_3$ Layers, with *n* as the Number of $SrRuO_3$ Monolayers (ML) and *m* as the Number of Repeats

sample name	$SrTiO_3$//[*n* ML $SrRuO_3$/2 ML $SrIrO_3$/2 ML $SrZrO_3]_m$	Curie T_C (K)
SRO	$[6/0/0]_1$	133
RI	$[4/2/0]_1$	~90
RIZ	$[4/2/2]_1$	90
5RIZ	$[5/2/2]_6$	113
6RIZ	$[6/2/2]_6$	124
10RIZ	$[10/2/2]_6$	134
sample name	$SrTiO_3$//[*n* ML $SrRuO_3$/2 ML $SrHfO_3$/2 ML $SrZrO_3]_m$	Curie T_C (K)
5RHZ	$[5/2/2]_6$	133
6RHZ	$[6/2/2]_6$	135

In Figure 2, we summarized an overview of the total Hall resistance hysteresis loops of the samples possessing $SrRuO_3/SrIrO_3$ interfaces as well as of a six monolayer (ML)-thick bare $SrRuO_3$ thin film studied as a reference sample (sample SRO in Table 1, see Figure 2a). The magnetic field was applied perpendicular to the sample surface for all Hall resistance measurements reported here. The trilayer RIZ, where we interfaced $SrRuO_3$ with $SrIrO_3$ on one side and capped it with $SrZrO_3$, shown in (c), is compared to the multilayer 5RIZ (see Figure 2d), which is a stacking of 6 times the trilayer (see Table 1 for their description).

The Hall resistivity, ρ_{xy}, of conventional ferromagnets is determined by two contributions, resulting from the ordinary Hall effect and the anomalous Hall effect,[16,17] usually scaling with the perpendicular applied magnetic field and the out-of-plane magnetization *M*, respectively. The scaling factors R_0 and R_s are the ordinary and anomalous Hall constants, respectively. Accordingly, the ordinary Hall constant, R_0, of the ferromagnetic thin films is determined by the slope of ρ_{xy} in the high magnetic field range, where the magnetization is saturated and the anomalous Hall resistivity is assumed to be field-independent. Typically, $SrRuO_3$ epitaxial layers exhibit a negative ordinary Hall constant, R_0, in a broad temperature range within the ferromagnetic phase, consistent with electron-dominated transport, as observed in bare $SrRuO_3$ thin films[18] and $SrRuO_3$-based multilayers[19] grown on $SrTiO_3$(100) substrates.

As the temperature increases, the anomalous Hall constant, R_s, of all of the investigated heterostructures has a complex temperature dependence and reverses sign from negative to positive at a sample-specific temperature, subsequently named T_{AHE}, which is usually close to the Curie temperature of $SrRuO_3$.

As we expect that the $SrRuO_3$ layers of the multilayers have an orthorhombic structure (confirmed by SAED patterns acquired at RT, Figure 1b,c), such behavior is in good agreement with the literature, where the nonmonotonous temperature dependence of R_s was observed[20−23] and also theoretically predicted[23] for orthorhombic $SrRuO_3$ single crystals and thin films. The change of R_s sign as a function of temperature was attributed to the dominant contribution of

https://dx.doi.org/10.1021/acsomega.9b03996
ACS Omega 2020, 5, 5824−5833

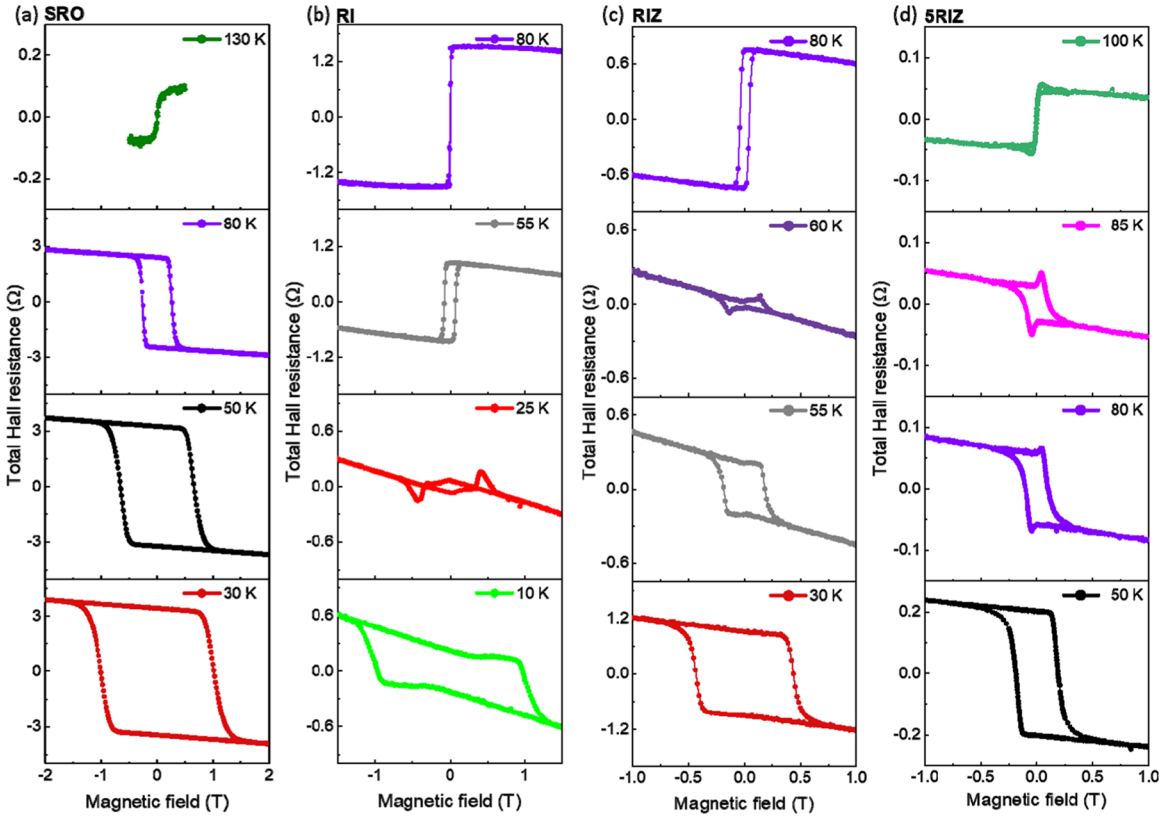

Figure 2. Hysteresis loops of the total Hall resistance at different temperatures for (a) 6 ML bare $SrRuO_3$ (SRO), (b) bilayer sample RI (4 ML $SrRuO_3$/2 ML $SrIrO_3$), (c) trilayer sample RIZ (4 ML $SrRuO_3$/2 ML $SrIrO_3$/2 ML $SrZrO_3$), and (d) multilayer sample 5RIZ ([5 ML $SrRuO_3$/2 ML $SrIrO_3$/2 ML $SrZrO_3$]$_6$), capturing the change of sign of the anomalous Hall effect around a sample-specific temperature, T_{AHE}.

the intrinsic AHE mechanism. The total Berry curvature changes due to the Fermi level shift around the crossing points of the conduction band through the temperature scan and results in the change of sign of the intrinsic AHE conductivity.[23−26]

The anomalous Hall constant, R_s, of the 6 ML bare $SrRuO_3$ film (sample SRO) reverses its sign a little below 130 K (see Figure 2a), close to the Curie temperature. In contrast, T_{AHE} was decreased for the heterostructures exhibiting $SrRuO_3$/$SrIrO_3$ interfaces, accompanied by the reduction of the ferromagnetic transition temperature (see Table 1 for further details). For the bilayer RI, T_{AHE} was about 25 K (Figure 2b, second panel from the top). T_{AHE} was about 60 K for the RIZ trilayer (see Figure 2c, second panel from the top) and about 90 K (Figure 2d, second panel from the top) for the multilayer 5RIZ. These important variations of T_{AHE} stress that not only the individual $SrRuO_3$ layer thickness determines the AHE behavior but also the particular interfaces and sample configurations play central roles. The oxygen octahedra tilts may be slightly different for the $SrRuO_3$ layer in the case of the RI and RIZ samples due to the extra capping of the sample RIZ with 2 ML orthorhombic $SrZrO_3$ with large oxygen octahedral tilts. Recently, there have been reports that the inhomogeneity of the structure across $SrRuO_3$ layers, due to variations of the RuO_6 octahedral tilts, may result in inhomogeneous anomalous Hall conductivity and THE-like additional contributions to the AHE resistivity loops.[9,27]

The AHE resistance loops of the investigated bare $SrRuO_3$ sample (SRO) exhibited a square shape resembling closely the expected magnetization hysteresis of ferromagnetically hard $SrRuO_3$ epitaxial films when the magnetic field is applied close to the magnetic easy axis.[19] When $SrRuO_3$ layers were interfaced with layers of the large SOC $SrIrO_3$, peaklike features were observed for the AHE resistance loops of the heterostructures close to T_{AHE}. Such anomalies were absent for the bare $SrRuO_3$ film at any temperature down to 10 K, which agrees with previous magnetotransport studies of high-quality, orthorhombic $SrRuO_3$ thin films.[28] The peaklike anomalies were clearly present in the heterostructures between 10 and 25 K for the bilayer RI, whereas the temperature range was increased and shifted to higher temperatures, 50−60 K, for the trilayer RIZ and to 80−100 K for the 5RIZ superlattice. The AHE resistance loops of the RIZ and 5RIZ multilayers had a square shape at low temperatures only (see the loops measured at 30 or 50 K in Figure 2c,d).

In the last couple of years, similar anomalies of the AHE resistance loops were observed in a variety of bare $SrRuO_3$ ultrathin films or $SrRuO_3$-based heterostructures, and their origins were considered to be related to various mechanisms. A number of studies assigned these peaklike features to the manifestation of the topological Hall effect generated by the formation of skyrmions, when the magnetization is being reversed between the opposite saturation states.[4−6] However, such effects in the Hall resistivity and the formation of skyrmions were reported also for ultrathin $SrRuO_3$ films interfaced with the ferroelectric $BaTiO_3$. The DMI in the absence of a 5d ion with strong spin−orbit coupling at the $SrRuO_3$/$BaTiO_3$ interface[29] was related to the ferroelectric off-centering of the ions at the interface. Recently, similar THE-like contributions were observed in bare $SrRuO_3$ thin films grown under nonoptimal conditions[30,31] or after postdeposition protonation,[32] as well. Alternative interpretations for the

https://dx.doi.org/10.1021/acsomega.9b03996
ACS Omega 2020, 5, 5824−5833

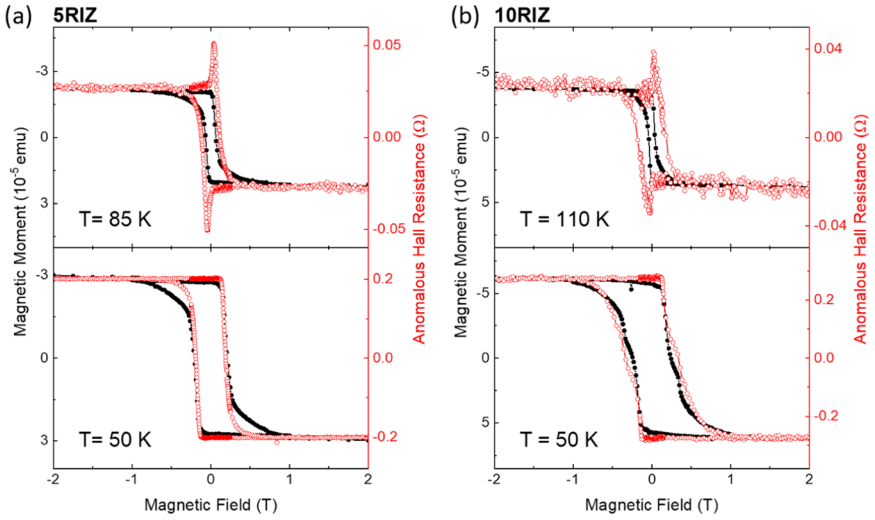

Figure 3. Comparison between the anomalous Hall resistance and the magnetic moment loops for (a) sample 5RIZ [5 ML $SrRuO_3$/2 ML $SrIrO_3$/2 ML $SrZrO_3$]$_6$ and for (b) sample 10RIZ [10 ML $SrRuO_3$/2 ML $SrIrO_3$/2 ML $SrZrO_3$]$_6$ at temperatures close to T_{AHE} and much below T_{AHE} (at 50 K). For the sake of comparison with the Hall loops, the *y* axis for the magnetic moment loops has inverted values.

origin of these anomalies take into account that the electronic conduction bands of $SrRuO_3$, which exhibits multiple Weyl nodes in proximity to the Fermi level, are strongly dependent on external perturbations and on temperature. The Berry curvature of these topologically nontrivial bands determines the intrinsic contribution to the anomalous Hall conductivity, which is considered to be the dominant asymmetric scattering mechanism in the case of $SrRuO_3$.[8] Therefore, the origins of the observed anomalies in the Hall resistivity of $SrRuO_3$-based heterostructures were assigned to changes in the band structure of $SrRuO_3$ induced by defects such as Ru vacancies or H implantation,[30,32] to inhomogeneity because of domains with a distribution of coercive fields and of anomalous Hall constants,[8] to interface-induced electronic effects,[10] or to structural inhomogeneity.[9,27]

Moreover, very similar peaklike anomalies of the Hall loops were recently reported for other epitaxial films of ferromagnetic oxides, such as the n-doped $EuTiO_3$ (by La substitution of Eu) epitaxial films.[33] Nonmonotonic magnetic field dependence of the anomalous Hall resistivity was measured, which was ascribed to the change of electronic bands induced by Zeeman splitting during the magnetization process. The anomalous Hall resistivity measurement in La-doped $EuTiO_3$ films showed additional terms in the AHE during the magnetization process, which were not proportional to the magnetization. Theoretical calculations indicated that the change of the Zeeman field in the process of canting the magnetic moments causes a shift of the Weyl nodes in the conduction bands, resulting in a peculiar magnetic field dependence of the AHE, closely resembling an additional THE contribution. In contrast to n-doped $EuTiO_3$ films, it is hard to expect that doping of $SrRuO_3$ due to either charge transfer at $SrRuO_3$/$SrIrO_3$ interfaces[34] or to Ir substitution of Ru in $SrRuO_3$ films can tune the position of the Fermi level around the conduction band crossings strongly because $SrRuO_3$ typically has a large density of charge carriers. However, ultrathin $SrRuO_3$ films such as in our heterostructures have lower electron densities. Moreover, in ABO_3 perovskites, B-site substitutions may result in distortions of the B−O−B bond angles and lengths, thereby affecting the structural symmetry and consequently the band structure. We therefore consider as a plausible explanation that Ir replacement of Ru in the $SrRuO_3$ due to intermixing at $SrRuO_3$/$SrIrO_3$ interfaces may cause a similar effect on the anomalous Hall conductivity such as that observed for the La-doped $EuTiO_3$ films.

In addition, oxygen ions might migrate across the interfaces, as it has been observed in ferromagnet/oxide heterostructures.[35,36] This would induce oxygen vacancies in one layer and oxygen excess in the neighboring layer, which can influence the electronic properties of the $SrRuO_3$-based heterostructures.[37] However, the oxygen surface exchange and the oxygen diffusion coefficients were found to be comparably small in $SrRuO_3$,[38] and here, we did not address the details of the stoichiometry of the layers by any techniques.

To test whether the AHE resistance loops were proportional to the magnetization loops and in which temperature range, in Figure 3, we compared the magnetic moment hysteresis loops determined from superconducting quantum interference device (SQUID) magnetometry measurements with the AHE resistance loops (after subtraction of the ordinary Hall effect linear contribution). We focused on comparing the data for the multilayers 5RIZ and 10RIZ, with 5 ML-thick $SrRuO_3$ and 10 ML-thick $SrRuO_3$, respectively. In high magnetic fields (larger than 1 T), as the magnetization of the multilayers was saturated, the anomalous Hall resistance appeared to be proportional to the magnetization. Below 50 K, for the 5RIZ multilayer, the coercive field of the magnetic moment loops and the magnetic field for which the anomalous Hall resistance is zero are in good agreement, within the measurement accuracy. At temperatures close to T_{AHE} (at 85 K for sample 5RIZ and at 110 K for sample 10RIZ, see Figure 3, upper panels), the AHE resistance loops exhibit peaks, when, starting from a saturated state, the magnetization direction starts reversing in the applied magnetic field of opposite polarity. The magnetic moment hysteresis loops (black full symbol curves in Figure 3) do not show such peaklike features. The assumption of direct proportionality of the anomalous Hall resistance to the magnetization[23] fails to describe the AHE resistance loops in this particular case, whereas it describes fairly well the AHE resistance loops of the SRO sample (see Figure S7, Supporting Information). Additionally, especially for

https://dx.doi.org/10.1021/acsomega.9b03996
ACS Omega 2020, 5, 5824−5833

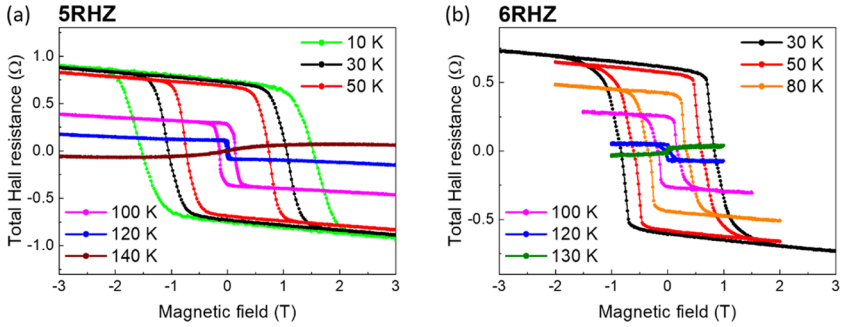

Figure 4. Magnetic field dependence of the total Hall resistance at various temperatures for the two multilayers with $SrRuO_3$ layers interfaced with the large band gap insulators $SrHfO_3$ and $SrZrO_3$: (a) multilayer 5RHZ (with 5 ML-thick $SrRuO_3$) and (b) multilayer 6RHZ (with 6 ML-thick $SrRuO_3$).

the measurements of sample 10RIZ at 110 K (Figure 3b, upper panel), the value of the coercive field for the magnetic moment loops and the value at which the AHE resistance is zero in the AHE loops are dramatically different. Even at lower temperatures, in the absence of any peaklike features (see the lower panel of Figure 3), discrepancies in the magnetic field dependence of the magnetization and the anomalous Hall resistance are present in the intermediate field range before reaching the saturation of the magnetization. We note here that the measurements summarized in Figure 3 were performed in different experimental setups (SQUID magnetometer for the magnetic moment loops and physical property measurement system (PPMS) for the AHE loops) so that slight differences in the measurement temperature and also the effect of different ways how the magnetic field was varied during running the hysteresis measurements could not be ruled out (see the Supporting Information for further discussion).

We stress out that according to the experimental results and the theoretical calculations from ref 4, an effective DMI should vanish in bilayers with $SrRuO_3$ layers thicker than seven ML and thus no contribution from an interface-driven THE should be observed any longer. However, peaklike contributions of similar shape are also observed in the AHE of our 10RIZ heterostructure that has 10 ML-thick $SrRuO_3$ layers. This indicates that either the upper limit of 7 ML-thick $SrRuO_3$ layer for the $SrRuO_3/SrIrO_3$ interfaces was an invalid prediction[4] or the effective interfacial DMI is larger for $SrRuO_3$ layers in our 10RIZ multilayers or the peaklike structures have nothing to do with interfacial DMI. Therefore, we ought to look for alternative explanations for the unconventional features of the AHE resistivity loops of the samples with $SrRuO_3/SrIrO_3$ interfaces. One possibility is the existence of inhomogeneity within the $SrRuO_3$ layers, exhibiting a distribution of coercive fields, AHE constants, R_s, and temperatures at which the AHE changes sign, T_{AHE}. Considering the procedure proposed by Kan et al.,[8] the general trend of the AHE curves can be reproduced under the assumption of a Gaussian distribution of sample regions possessing the temperature T_i (see Figure S9, Supporting Information).

Another explanation may be that the anomalous Hall effect in $SrRuO_3$ is dominated by the intrinsic mechanism due to the nontrivial topology of some electronic conduction bands, with multiple Weyl nodes. Effective intermixing of ordinary and anomalous Hall effect was observed by Roy et al.[39] In ref 39, it was concluded that the AHE resistivity of $SrRuO_3$ films cannot be described as a sum of a term that depends linearly on the magnetic field and a term that depends linearly on magnetization. This was attributed to the dependence of the Weyl node contribution to the intrinsic AHE conductivity on the magnetic field and the magnetization.

Imaging of the magnetic domains is very helpful to elucidate whether the formation of skyrmions is a viable explanation. Matsuno et al.[4] and more recently Meng et al.[6] performed magnetic force microscopy (MFM) investigations of the domains in $SrRuO_3/SrIrO_3$ bilayers and found small bubblelike domains, which formed in the temperature and magnetic field range for which the AHE resistivity loops exhibited the peaklike features. However, here, we have multilayers with many repeats of the $SrRuO_3/SrIrO_3$, and in a previous study on the magnetic interlayer coupling, we demonstrated that $SrRuO_3$ layers separated by $SrIrO_3/SrZrO_3$ spacers with a total thickness of 2−4 ML are only very weakly ferromagnetically coupled.[40] This rendered very difficult our attempts to investigate the domains by MFM for the multilayers studied here as the nucleation of domains occurred independently in the individual $SrRuO_3$ layers of the multilayers and the magnetization switching process proceeded independently in the six layers. The MFM measurements confirmed that the layers are decoupled by observing that at many sites switching of the local magnetization occurred six times for a multilayer with six $SrRuO_3$ layers. Consequently, no conclusive information on the formation of skyrmions could be derived from our MFM investigations of the multilayers with decoupled ferromagnetic layers (e.g., sample 5RIZ). MFM measurements performed on the asymmetric heterostructure RIZ that has a single $SrRuO_3$ layer allowed, however, unambiguous imaging of the magnetic domains. The summary of the MFM study of the RIZ sample can be found in the preprint by Malsch et al.[41] The MFM investigations of RIZ sample did not indicate the formation of skyrmions in the temperature and magnetic field range where peaklike anomalies were present in the AHE resistivity loops (see, for example, Figure 2c, 55−60 K). The hump features of the AHE loops started to develop at values of the magnetic field where, in the MFM experiments, the magnetization was not yet changing as no observable nucleation of domains was occurring. For example, at 55 K, in the prior saturated $SrRuO_3$ layer (in a field of 2 T), the first domains of reversed magnetization appear to nucleate at fields larger than −95 mT, whereas the humps of the corresponding AHE loops start developing at much lower fields.[41] Inhomogeneities of the $SrRuO_3$ layer due to one unit cell thickness variation along the

https://dx.doi.org/10.1021/acsomega.9b03996
ACS Omega 2020, 5, 5824−5833

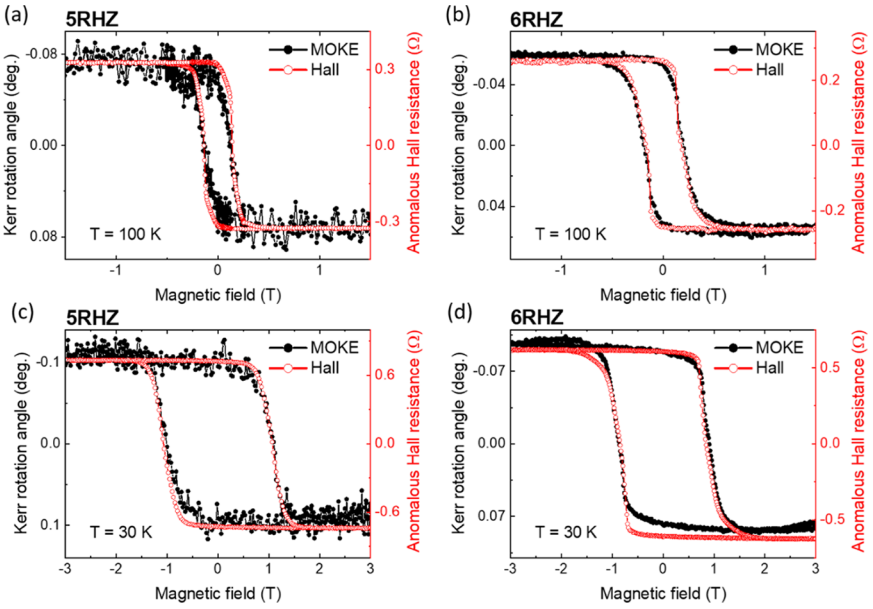

Figure 5. Anomalous Hall resistance loops (red open symbols) and the Kerr rotation angle loops (black full symbols), measured simultaneously for sample 5RHZ and sample 6RHZ, at 100 K ((a) for 5RHZ, (b) for 6RHZ) and at 30 K ((c) for 5RHZ, (d) for 6RHZ). For the sake of comparison with the Hall loops, the *y* axis for the Kerr loops has inverted values.

terrace ledges were found to affect the local switching fields and suggested to impact the global coercive fields.

To get more insight into the role played by the interfacing of $SrRuO_3$ with $SrIrO_3$ (with large SOC $5d^5$ Ir^{4+} ions), we fabricated multilayers in which the large band gap insulator $SrHfO_3$ ($5d^0$ Hf^{4+} ions) layers substituted the $SrIrO_3$ layers (see microstructure investigations in Figure 1f–h and details of the samples in Table 1). The total Hall resistance loops of the samples 5RHZ and 6RHZ are shown in Figure 4. In contrast to the multilayers possessing $SrRuO_3/SrIrO_3$ interfaces, the anomalous Hall resistance of the multilayers with $SrRuO_3/SrHfO_3$ interfaces behaved rather conventionally: the AHE loops did not show any peaklike anomalies resembling THE contributions. As typical for $SrRuO_3$, the sign of AHE was negative for the 5RHZ multilayer up to 120 K (Figure 4a). For the 6RHZ multilayer, the sign of the AHE changed from negative to positive at about 130 K, in close vicinity of the Curie temperature of the sample (see Figure 4b). Anomalous Hall resistance loops from which the ordinary Hall contribution was subtracted were compared with the Kerr rotation angle loops and are shown in Figure 5. The Kerr rotation angle is assumed to be proportional to the perpendicular component of the total heterostructure magnetization. We emphasize here that the Hall and magneto-optic Kerr effect (MOKE) measurements were performed in the same setup simultaneously, ensuring identical measurement conditions in view of temperature and external magnetic field orientation (further details can be found in the Supporting Information).

For the heterostructures with $SrRuO_3/SrHfO_3$ interfaces, the anomalous Hall resistance can be described by considering the total thin film magnetization and an AHE constant, R_s, that is independent of the magnetic field. However, we point out here that small deviations in the magnetic field dependence of MOKE response and Hall resistance are still present due to the imperfect corrections of the background, substrate, and impurity contributions, affecting the loops measured by each technique (see also the discussion in the Supporting Information, concerning background corrections of the SQUID loops, Figure S4). Often, the anomalous Hall resistance is calculated by taking input parameters from the measured MOKE loops[4,5] or a predicted magnetization loop,[42] but the correction of the loops is not made available for the readership. Subtracting thus-derived anomalous Hall resistance loops from the total Hall resistance loops will generate a nonzero result, even for loops without obvious peaklike anomalies. This should be taken into account when magneto-transport measurements are used exclusively to investigate the existence of skyrmions.

Compared to the $SrRuO_3/SrIrO_3/SrZrO_3$ multilayers, the dislocation density of the $SrRuO_3/SrHfO_3/SrZrO_3$ multilayers is higher and clear variations in $SrRuO_3$ layer thickness were observed in the HAADF-STEM investigations (summarized in Figure 1). If structural defects or $SrRuO_3$ layer thickness variations resulted in the deterioration of the physical properties of the multilayers, the effect would be expected to be more pronounced in the heterostructures possessing $SrRuO_3/SrHfO_3$ interfaces. However, we point out first that the Curie temperature of the multilayers with $SrHfO_3$ is considerably larger than that of the multilayers with $SrIrO_3$ (see Table 1 and Figure S5, Supporting Information). Furthermore, if thickness variation of the individual $SrRuO_3$ layers across the multilayers was the dominant cause for the observed anomalies of the AHE resistance loops,[43] these anomalies should occur also for the multilayers with $SrHfO_3$. We also stress out that as all of the heterostructures were grown under the same pulsed laser deposition (PLD) conditions, we assume that the stoichiometry of the $SrRuO_3$ layers is very similar for the two types of multilayers, and hence, the possibility that Ru vacancies resulted in the observed peaklike anomalies[30] can be ruled out for our samples. However, it may be that intermixing at $SrRuO_3/SrHfO_3$ interfaces that resulted in Hf replacing Ru had a benign effect on the electronic band structure of the $SrRuO_3$, unlike the replacement of Ru with Ir at $SrRuO_3/SrIrO_3$

https://dx.doi.org/10.1021/acsomega.9b03996
ACS Omega 2020, 5, 5824−5833

interfaces. However, we have not had so far the opportunity to analyze the intermixing issues quantitatively.

3. CONCLUSIONS

In conclusion, interfacing ferromagnetic $SrRuO_3$ layers with 5d perovskite oxides possessing large spin−orbit coupling has been proposed as a route to generate interfacial Dzyaloshinskii−Moriya interaction, which can result in the formation of noncollinear magnetic texture and even ultrasmall skyrmions. Here, the magnetic and magnetotransport properties of ultrathin $SrRuO_3$ asymmetric heterostructures with 5d perovskites were investigated and compared to those of a bare $SrRuO_3$ film of a similar thickness. For $SrRuO_3$ layers interfaced with $SrIrO_3$ ($5d^5$ Ir^{4+} ions), unconventional features appear in the field dependence of the anomalous Hall resistance. The substitution of the paramagnetic semimetal $SrIrO_3$ by the band insulator $SrHfO_3$ ($5d^0$ Hf^{4+} ions) resulted in drastic changes in the anomalous Hall resistance loops of the $SrRuO_3$ layers and also the global magnetic properties. The ferromagnetic Curie temperature and the temperature at which anomalous Hall constant, R_s, changes from negative to positive values were larger for the multilayers with $SrHfO_3$. The Hall resistivity loops of the heterostructures with $SrRuO_3/SrHfO_3$ interfaces can be described by a term that is linear in the magnetic field and a term that is linear in magnetization and do not show any unconventional behavior as, for instance, peaklike features. Our microstructural investigations, showing an increased defect density for the multilayers with $SrRuO_3/SrHfO_3$ interfaces, indicate that the anomalies observed for the heterostructures possessing $SrRuO_3/SrIrO_3$ interfaces might originate in our case from electronic inhomogeneity of the $SrRuO_3$ layers rather than from structural defects or thickness variation. We are reluctant to consider that skyrmions could be at the origin of the THE-like humps because MFM investigations of the RIZ sample (with a single $SrRuO_3/SrIrO_3$ interface) did not reveal the formation of any domains resembling skyrmions. The precise microscopic mechanism driving the occurrence of the anomalies in the Hall resistance loops is still to be determined and requires more input from theoretical calculations of the band structure for $SrRuO_3/SrIrO_3$ and $SrRuO_3/SrHfO_3$ bilayers of similar thickness as under study here. However, our results highlight the importance of the details of interfacial interactions and structural modifications of epitaxial $SrRuO_3$ with a central role being played most likely by the interactions with the large spin−orbit coupling $5d^5$ Ir^{4+} ions.

4. MATERIALS AND EXPERIMENTAL METHODS

The samples (see the summary in Table 1) were fabricated by pulsed laser deposition (PLD) with a KrF excimer laser using stoichiometric targets of $SrRuO_3$, $SrIrO_3$, $SrZrO_3$, and $SrHfO_3$. The epitaxial layers were deposited on (100) $SrTiO_3$ single-crystal substrates that were etched in NH_4F-buffered HF solution for 2−2.5 min and annealed in air at 1000 °C for 2 h. The substrate temperature was 650 °C and the partial oxygen pressure was 0.133 mbar for the growth of all of the layers. The laser fluence was about 1.5 J/cm^2 for the ablation of all materials, and the pulse repetition rate of the laser was 5 Hz for the $SrRuO_3$ layers and 1−2 Hz for all of the other materials.

The deposition was monitored by reflective high-energy electron diffraction (RHEED) (see Figure S1a−c, Supporting Information) under high oxygen pressure to observe the growth mode and control the thicknesses of the $SrZrO_3$, $SrIrO_3$, $SrHfO_3$ layers, which grew in a layer-by-layer growth mode. For all of the compounds grown here, a monolayer (ML) is about 0.4 nm thick. To ensure the stoichiometric oxygen content of the layers, the heterostructures were cooled down at a rate of 10 °C/min, in an oxygen atmosphere of 200 mbar. The morphologies of the STO substrates and heterostructures were observed by atomic force microscopy (see Figure S1d−f, Supporting Information). Scanning transmission electron microscopy (STEM) of cross-sectional specimens was conducted to investigate the microstructure of the multilayers and their interfaces. High-angle annular dark-field (HAADF)-STEM imaging and energy-dispersive X-ray spectroscopy (EDXS) were performed with an FEI Titan 80200 ChemiSTEM microscope. HAADF-STEM imaging enabled us to determine the thickness of the individual layers and compare the values with those expected based on RHEED data. The magnetization of the heterostructures, as a function of temperature and magnetic field, was measured with a superconducting quantum interference device (SQUID) magnetometer (MPMS XL7 from Quantum Design). Magnetic background measurements of the diamagnetic $SrTiO_3$ substrates were performed and subtracted from the total magnetic response (see the Supporting Information).

Hall effect measurements were carried out in the four-point van der Pauw geometry with permutating contacts for antisymmetrization. Hall resistivity loops were recorded both with a physical property measurement system (PPMS, Quantum Design, Inc.) and with a homemade setup enabling the simultaneous measurement of the transverse Hall resistance and magneto-optic Kerr effect (MOKE). The polar MOKE studies were performed with the magnetic field applied perpendicular to the thin film surface by utilizing incoherent light. The probe wavelength was chosen individually for each sample to reduce optical artifacts like interference effects that can be present in ultrathin films of $SrRuO_3$. In the case of the MOKE investigations of the samples 5RHZ and 6RHZ, incoherent light of 650 nm wavelength was used.

■ ASSOCIATED CONTENT

Supporting Information

The Supporting Information is available free of charge at https://pubs.acs.org/doi/10.1021/acsomega.9b03996.

Sample fabrication and structural characterization details, SQUID magnetometry-background correction, determination of ferromagnetic transition temperature, polar MOKE measurement details, properties of bare 6 ML-thick $SrRuO_3$ film, and theoretical description of the AHE resistance loops of electrically inhomogeneous layers (PDF)

■ AUTHOR INFORMATION

Corresponding Author

Ionela Lindfors-Vrejoiu − *Institute of Physics II, University of Cologne, 50937 Cologne, Germany*; orcid.org/0000-0003-3196-7313; Email: vrejoiu@ph2.uni-koeln

Authors

Lena Wysocki − *Institute of Physics II, University of Cologne, 50937 Cologne, Germany*

https://dx.doi.org/10.1021/acsomega.9b03996
ACS Omega 2020, 5, 5824−5833

Jörg Schöpf − *Institute of Physics II, University of Cologne, 50937 Cologne, Germany*
Michael Ziese − *Felix Bloch Institute for Solid State Physics, University of Leipzig, 04109 Leipzig, Germany*
Lin Yang − *Institute of Physics II, University of Cologne, 50937 Cologne, Germany*
András Kovács − *Ernst Ruska-Centre for Microscopy and Spectroscopy with Electrons, Forschungszentrum Jülich GmbH, 52425 Jülich, Germany*
Lei Jin − *Ernst Ruska-Centre for Microscopy and Spectroscopy with Electrons, Forschungszentrum Jülich GmbH, 52425 Jülich, Germany;* orcid.org/0000-0001-6924-2364
Rolf B. Versteeg − *Institute of Physics II, University of Cologne, 50937 Cologne, Germany*
Andrea Bliesener − *Institute of Physics II, University of Cologne, 50937 Cologne, Germany*
Felix Gunkel − *PGI-7, Forschungszentrum Jülich, 52428 Jülich, Germany; Institute of Electronic Materials (IWE2), RWTH Aachen University, 52062 Aachen, Germany*
Lior Kornblum − *Andrew & Erna Viterbi Department of Electrical Engineering, Technion—Israel Institute of Technology, 3200003 Haifa, Israel;* orcid.org/0000-0001-6305-7619
Regina Dittmann − *PGI-7, Forschungszentrum Jülich, 52428 Jülich, Germany*
Paul H. M. van Loosdrecht − *Institute of Physics II, University of Cologne, 50937 Cologne, Germany;* orcid.org/0000-0002-3704-9890

Complete contact information is available at: https://pubs.acs.org/10.1021/acsomega.9b03996

Author Contributions

This research study was designed and supervised by I.L.-V. L.W. and I.L.-V. fabricated the samples. L.W. performed SQUID magnetometry and part of the Hall measurements and the data analyses. J.S. constructed the MOKE−Hall set up and together with L.Y. performed the Hall and the MOKE measurements and corresponding data analyses. M.Z. performed some of the Hall and SQUID measurements and gave valuable advice for further investigations. STEM and TEM investigations were carried out by A.K. and L.J. R.B.V. and P.H.M.v.L. supervised the MOKE−Hall setup construction and the MOKE experiments and were involved in regular discussions. A.B. performed AFM and helped with some of the Hall measurements by PPMS. F.G. and R.D. assisted the sample fabrication and structural characterization at FZ Jülich and participated in helpful discussions. L.K. performed X-ray diffraction (XRD) and analyzed the data. The manuscript was written by L.W. and I.L.-V. with significant contributions of all authors. All authors have given approval to the final version of the manuscript.

Notes

The authors declare no competing financial interest.

■ ACKNOWLEDGMENTS

The authors thank René Borowski (FZ Jülich) for etching the substrates, and Alexey Taskin and Susanne Heijligen (University of Cologne) for assistance with PPMS and SQUID measurements. Insightful suggestions from Stefan Blügel and Marjana Lezaic (FZ Jülich), from Achim Rosch (University of Cologne) and Carmine Autieri (Polish Academy of Sciences), are gratefully acknowledged. The authors are thankful to Peter Milde, Dmytro Ivaneiko, and Lukas Eng (Technical University Dresden) for MFM investigations and Maria Baskin (Technion) for assistance with XRD-reciprocal space mapping (RSM). Financial support from the German Research Foundation (projects LI3015/3-1 (No. 335038432), LI3015/5-1 (No. 403504808 within SPP 2137)), from CRC1238 (No. 277146847), and from the German Excellence Initiative via the key profile area "quantum matter and materials" (QM2) of the University of Cologne is gratefully acknowledged.

■ ABBREVIATIONS

SOCspin−orbit coupling; DMIDzyaloshinskii−Moriya interaction; AHEanomalous Hall effect; THEtopological Hall effect; SQUIDsuperconducting quantum interference device; MOKEmagneto-optic Kerr effect; PLDpulsed laser deposition; RHEEDreflective high-energy electron diffraction; HAADF-STEMhigh-angle annular dark-field scanning transmission electron microscopy; SAEDselective area electron diffraction; EDXSenergy-dispersive X-ray spectroscopy; MLmonolayer

■ REFERENCES

(1) Yi, D.; Liu, J.; Hsu, S.-L.; Zhang, L.; Choi, Y.; Kim, J.-W.; Chen, Z.; Clarkson, J. D.; Serrao, C. R.; Arenholz, E.; Ryan, P. J.; Xu, H.; Birgeneau, R. J.; Ramesh, R. Atomic-Scale Control of Magnetic Anisotropy via Novel Spin−orbit Coupling Effect in $La_{2/3}$ $Sr_{1/3}MnO_3$ /$SrIrO_3$ Superlattices. *Proc. Natl. Acad. Sci. U.S.A.* **2016**, *113*, 6397−6402.
(2) Nichols, J.; Gao, X.; Lee, S.; Meyer, T. L.; Freeland, J. W.; Lauter, V.; Yi, D.; Liu, J.; Haskel, D.; Petrie, J. R.; Guo, E.-J.; Herklotz, A.; Lee, D.; Ward, T. Z.; Eres, G.; Fitzsimmons, M. R.; Lee, H. N. Emerging Magnetism and Anomalous Hall Effect in Iridate-Manganite Heterostructures. *Nat. Commun.* **2016**, *7*, No. 12721.
(3) Pang, B.; Zhang, L.; Chen, Y. B.; Zhou, J.; Yao, S.; Zhang, S.; Chen, Y. Spin-Glass-like Behavior and Topological Hall Effect in $SrRuO_3$ - $SrIrO_3$ Superlattices for Oxide Spintronics Applications. *ACS Appl. Mater. Interfaces* **2017**, *9*, 3201−3207.
(4) Matsuno, J.; Ogawa, N.; Yasuda, K.; Kagawa, F.; Koshibae, W.; Nagaosa, N.; Tokura, Y.; Kawasaki, M. Interface-Driven Topological Hall Effect in $SrRuO_3$/ $SrIrO_3$ Bilayer. *Sci. Adv.* **2016**, *2*, No. e1600304.
(5) Ohuchi, Y.; Matsuno, J.; Ogawa, N.; Kozuka, Y.; Uchida, M.; Tokura, Y.; Kawasaki, M. Electric-Field Control of Anomalous and Topological Hall Effects in Oxide Bilayer Thin Films. *Nat. Commun.* **2018**, *9*, No. 213.
(6) Meng, K.-Y.; Ahmed, A. S.; Bacani, M.; Mandru, A.-O.; Zhao, X.; Bagués, N.; Esser, B. D.; Flores, J.; McComb, D. W.; Hug, H. J.; Yang, F. Observation of Nanoscale Skyrmions in $SrIrO_3$/$SrRuO_3$ Bilayers. *Nano Lett.* **2019**, *19*, 3169−3175.
(7) Taguchi, Y.; Oohara, Y.; Yoshizawa, H.; Nagaosa, N.; Tokura, Y. Spin Chirality, Berry Phase, and Anomalous Hall Effect in a Frustrated Ferromagnet. *Science* **2001**, *291*, 2573−2576.
(8) Kan, D.; Moriyama, T.; Kobayashi, K.; Shimakawa, Y. Alternative to the Topological Interpretation of the Transverse Resistivity Anomalies in $SrRuO_3$. *Phys. Rev. B* **2018**, *98*, No. 180408(R).
(9) Ziese, M.; Jin, L.; Lindfors-Vrejoiu, I. Unconventional Anomalous Hall Effect Driven by Oxygen-Octahedra-Tailoring of the $SrRuO_3$ Structure. *J. Phys. Mater.* **2019**, *2*, No. 034008.
(10) Groenendijk, D. J.; Autieri, C.; van Thiel, T. C.; Brzezicki, W.; Gauquelin, N.; Barone, P.; van den Bos, K. H. W.; van Aert, S.; Verbeeck, J.; Filippetti, A.; Picozzi, S.; Cuoco, M.; Caviglia, A. D. Berry phase engineering at oxide interfaces 2018, arXiv:1810.05619. arXiv.org e-Print archive. https://arxiv.org/abs/1810.05619.
(11) Moreau-Luchaire, C.; Moutafis, C.; Reyren, N.; Sampaio, J.; Vaz, C. A. F.; Van Horne, N.; Bouzehouane, K.; Garcia, K.; Deranlot, C.; Warnicke, P.; Wohlhüter, P.; George, J.-M.; Weigand, M.; Raabe, J.; Cros, V.; Fert, A. Additive Interfacial Chiral Interaction in

Multilayers for Stabilization of Small Individual Skyrmions at Room Temperature. *Nat. Nanotechnol.* **2016**, *11*, 444−448.
(12) Wang, L.; Liu, C.; Mehmood, N.; Han, G.; Wang, Y.; Xu, X.; Feng, C.; Hou, Z.; Peng, Y.; Gao, X.; Yu, G. Construction of a Room-Temperature Pt/Co/Ta Multilayer Film with Ultrahigh-Density Skyrmions for Memory Application. *ACS Appl. Mater. Interfaces* **2019**, *11*, 12098−12104.
(13) Kennedy, B. J.; Howard, C. J.; Chakoumakos, B. C. High-Temperature Phase Transitions in $SrZrO_3$. *Phys. Rev. B* **1999**, *59*, 4023−4027.
(14) Sawkar-Mathur, M.; Marchiori, C.; Fompeyrine, J.; Toney, M. F.; Bargar, J.; Chang, J. P. Structural Properties of Epitaxial $SrHfO_3$ Thin Films on Si (001). *Thin Solid Films* **2010**, *518*, S118−S122.
(15) Biswas, A.; Jeong, Y. H. Growth and Engineering of Perovskite $SrIrO_3$ Thin Films. *Curr. Appl. Phys.* **2017**, *17*, 605−614.
(16) Pugh, E. M.; Rostoker, N. Hall Effect in Ferromagnetic Materials. *Rev. Mod. Phys.* **1953**, *25*, 151−157.
(17) Nagaosa, N.; Sinova, J.; Onoda, S.; MacDonald, A. H.; Ong, N. P. Anomalous Hall Effect. *Rev. Mod. Phys.* **2010**, *82*, 1539−1592.
(18) Ziese, M.; Vrejoiu, I. Anomalous and Planar Hall Effect of Orthorhombic and Tetragonal $SrRuO_3$ Layers. *Phys. Rev. B* **2011**, *84*, No. 104413.
(19) Bern, F.; Ziese, M. Magnetotransport and Hall Effect Studies of $SrRuO_3$ / $SrTiO_3$ Superlattices. *EPJ Web Conf.* **2013**, *40*, No. 15013.
(20) Izumi, M.; Nakazawa, K.; Bando, Y.; Yoneda, Y.; Terauchi, H. Magnetotransport of $SrRuO_3$ Thin Film on $SrTiO_3$ (001). *J. Phys. Soc. Jpn.* **1997**, *66*, 3893−3900.
(21) Klein, L.; Reiner, J. R.; Geballe, T. H.; Beasley, M. R.; Kapitulnik, A. Extraordinary Hall Effect in $SrRuO_3$. *Phys. Rev. B* **2000**, *61*, No. R7842(R).
(22) Schultz, M.; Reiner, J. W.; Klein, L. The Extraordinary Hall Effect of $SrRuO_3$ in the Ultrathin Limit. *J. Appl. Phys.* **2009**, *105*, No. 07E906.
(23) Fang, Z.; Nagaosa, N.; Takahashi, K. S.; Asamitsu, A.; Mathieu, R.; Ogasawara, T.; Yamada, H.; Kawasaki, M.; Tokura, Y.; Terakura, K. The Anomalous Hall Effect and Magnetic Monopoles in Momentum Space. *Science* **2003**, *302*, 92−95.
(24) Mathieu, R.; Asamitsu, A.; Yamada, H.; Takahashi, K. S.; Kawasaki, M.; Fang, Z.; Nagaosa, N.; Tokura, Y. Scaling of the Anomalous Hall Effect in $Sr_{1-x}Ca_xRuO_3$. *Phys. Rev. Lett.* **2004**, *93*, No. 016602.
(25) Wang, X.; Vanderbilt, D.; Yates, J. R.; Souza, I. Fermi-Surface Calculation of the Anomalous Hall Conductivity. *Phys. Rev. B* **2007**, *76*, No. 195109.
(26) Chen, Y.; Bergman, D. L.; Burkov, A. A. Weyl Fermions and the Anomalous Hall Effect in Metallic Ferromagnets. *Phys. Rev. B* **2013**, *88*, No. 125110.
(27) Gu, Y.; Wei, Y.-W.; Xu, K.; Zhang, H.; Wang, F.; Li, F.; Saleem, M. S.; Chang, C.-Z.; Sun, J.; Song, C.; Feng, J.; Zhong, X.; Liu, W.; Zhang, Z.; Zhu, J.; Pan, F. Interfacial Oxygen-Octahedral-Tilting-Driven Electrically Tunable Topological Hall Effect in Ultrathin $SrRuO_3$ Films. *J. Phys. D: Appl. Phys.* **2019**, *52*, No. 404001.
(28) Bern, F.; Ziese, M.; Dörr, K.; Herklotz, A.; Vrejoiu, I. Hall Effect of Tetragonal and Orthorhombic $SrRuO_3$ Films. *Phys. Status Solidi RRL* **2013**, *7*, 204−206.
(29) Wang, L.; Feng, Q.; Kim, Y.; Kim, R.; Lee, K. H.; Pollard, S. D.; Shin, Y. J.; Zhou, H.; Peng, W.; Lee, D.; Meng, W.; Yang, H.; Han, J. H.; Kim, M.; Lu, Q.; Noh, T. W. Ferroelectrically Tunable Magnetic Skyrmions in Ultrathin Oxide Heterostructures. *Nat. Mater.* **2018**, *17*, 1087−1094.
(30) Kan, D.; Shimakawa, Y. Defect-Induced Anomalous Transverse Resistivity in an Itinerant Ferromagnetic Oxide. *Phys. Status Solidi B* **2018**, *255*, No. 1800175.
(31) Qin, Q.; Liu, L.; Lin, W.; Shu, X.; Xie, Q.; Lim, Z.; Li, C.; He, S.; Chow, G. M.; Chen, J. Emergence of Topological Hall Effect in a $SrRuO_3$ Single Layer. *Adv. Mater.* **2019**, *31*, No. 1807008.
(32) Li, Z.; Shen, S.; Tian, Z.; Hwangbo, K.; Wang, M.; Wang, Y.; Bartram, F. M.; He, L.; Lyu, Y.; Dong, Y.; Wan, G.; Li, H.; Lu, N.; Zang, J.; Zhou, H.; Arenholz, E.; He, Q.; Yang, L.; Luo, W.; Yu, P. Reversible manipulation of the magnetic state in $SrRuO_3$ through electric-field controlled proton evolution. *Nat. Commun.* **2020**, *11*, No. 184.
(33) Takahashi, K. S.; Ishizuka, H.; Murata, T.; Wang, Q. Y.; Tokura, Y.; Nagaosa, N.; Kawasaki, M. Anomalous Hall Effect Derived from Multiple Weyl Nodes in High-Mobility $EuTiO_3$ Films. *Sci. Adv.* **2018**, *4*, No. eaar7880.
(34) Zhong, Z.; Hansmann, P. Band Alignment and Charge Transfer in Complex Oxide Interfaces. *Phys. Rev. X* **2017**, *7*, No. 011023.
(35) Feng, C.; Wang, S.; Yin, L.; Li, X.; Yao, M.; Yang, F.; Tang, X.; Wang, L.; Mi, W.; Yu, G. Significant Strain-Induced Orbital Reconstruction and Strong Interfacial Magnetism in TiNi(Nb)/Ferromagnet/Oxide Heterostructures via Oxygen Manipulation. *Adv. Funct. Mater.* **2018**, *28*, No. 1803335.
(36) Wang, S.; Yao, M.; Li, Z.; Feng, C.; Wang, L.; Tang, X.; Kang, P.; Zhang, B.; Mi, W.; Yu, G. Nitrogen Tuned Charge Redistribution and Orbital Reconfiguration in Fe/MgO Interface for Significant Interfacial Magnetism Tunability. *Adv. Funct. Mater.* **2019**, *29*, No. 1806677.
(37) Lu, W.; He, K.; Song, W.; Sun, C.-J.; Chow, G. M.; Chen, J.-S. Effect of Oxygen Vacancies on the Electronic Structure and Transport Properties of $SrRuO_3$ Thin Films. *J. Appl. Phys.* **2013**, *113*, No. 17E125.
(38) Schraknepper, H.; Bäumer, C.; Dittmann, R.; De Souza, R. A. Complex Behaviour of Vacancy Point-Defects in $SrRuO_3$ Thin Films. *Phys. Chem. Chem. Phys.* **2015**, *17*, 1060−1069.
(39) Roy, D.; Haham, N.; Reiner, J. W.; Shimshoni, E.; Klein, L. Intermixing of Ordinary and Anomalous Hall Effect in $SrRuO_3$. *Phys. Rev. B* **2015**, *92*, No. 235101.
(40) Wysocki, L.; Mirzaaghayev, R.; Ziese, M.; Yang, L.; Schöpf, J.; Versteeg, R. B.; Bliesener, A.; Engelmayer, J.; Kovács, A.; Jin, L.; Gunkel, F.; Dittmann, R.; van Loosdrecht, P. H. M.; Lindfors-Vrejoiu. Magnetic Coupling of Ferromagnetic $SrRuO_3$ Epitaxial Layers Separated by Ultrathin Non-Magnetic $SrZrO_3$/ $SrIrO_3$. *Appl. Phys. Lett.* **2018**, *113*, No. 192402.
(41) Malsch, G.; Ivaneyko, D.; Milde, P.; Wysocki, L.; Yang, L.; van Loosdrecht, P. H. M.; Lindfors-Vrejoiu, I.; Eng, L. M. Correlating the Nanoscale Structural, Magnetic and Magneto-Transport Properties in $SrRuO_3$-Based Perovskite Thin Films: Implications for Oxide Skyrmion Devices. *ACS Appl. Nano Mater.* **2020**, DOI: 10.1021/acsanm.9b01918.
(42) Sohn, B.; Kim, B.; Park, S. Y.; Choi, H. Y.; Moon, J. Y.; Choi, T.; Choi, Y. J.; Noh, T. W.; Zhou, H.; Chang, S. H.; Han, J. H.; Kim, C. Emergence of Robust 2D Skyrmions in $SrRuO_3$ Ultrathin Film without the Capping Layer 2018, arXiv:1810.01615. arXiv.org e-Print archive. http://arxiv.org/abs/1810.01615.
(43) Wu, L.; Zhang, Y. Artificial Topological Hall Effect Induced by Intrinsic Thickness Non-uniformity in Ultrathin $SrRuO_3$ Films. 2018, arXiv:1812.09847. arXiv.org e-Print archive. https://arxiv.org/abs/1812.09847.

https://dx.doi.org/10.1021/acsomega.9b03996
ACS Omega 2020, 5, 5824−5833